Non-intrusive polynomial chaos methods for uncertainty quantification in wave problems at high frequencies

Nabil El Mocayd[a,*], M Shadi Mohamed[b], Mohammed Seaid[c]

[a]*International Water Research Institute, University Mohammed VI Polytechnic, Benguerir, Morocco*
[b]*School of Energy, Geoscience, Infrastructure and Society, Heriot-Watt University, Edinburgh EH14 4AS, UK*
[c]*Department of Engineering, University of Durham, South Road, DH1 3LE, UK*

Abstract

Numerical solutions of wave problems are often influenced by uncertainties generated by a lack of knowledge of the input values related to the domain data and/or boundary conditions in the mathematical equations used in the modeling. Conventional methods for uncertainty quantification in modeling waves constitute severe challenges due to the high computational costs especially at high frequencies/wavenumbers. For a given accuracy and a high wavenumber it is necessary to perform a mesh convergence study by refining the discretization of the computational domain with an increased resolution, which leads to increasing the number of degrees of freedom at a much higher rate than the wavenumber. This effect also known as the pollution error often limits the computations to relatively small values of the wavenumber. To estimate the uncertainties, many model evaluations are required, but only a single surrogate model is created in the process. In the present work, we propose the use of a non-intrusive spectral projection applied to a finite element framework with enriched basis functions for the uncertainty quantification of waves at high frequencies. The method integrates (i) the partition of unity finite element method for effectively computing the solutions of waves at high frequencies; and (ii) a non-intrusive spectral projection for effectively propagating random wavenumbers that encode uncertainties in the wave problems. Compared to the conventional finite element methods, the proposed method is demonstrated to reduce the total cost of accurately computing uncertainties in waves with high values of the wavenumber. Numerical results are presented for two sets of numerical tests. First, the interference of plane waves in a squared domain and then a wave scattering by a circular cylinder are studied at high wavenumbers. Comparisons to the Monte Carlo simulations and the regression based polynomial chaos expansion confirm the computational effectiveness of the proposed approach.

Keywords: Uncertainty quantification; Non-intrusive spectral projection; Polynomial chaos; Helmholtz equation; Scattering waves; High frequency; Partition of unity method; Finite element method.

*Corresponding author
Email addresses: nabil.elmocayd@um6p.ma (Nabil El Mocayd), m.s.mohamed@hw.ac.uk (M Shadi Mohamed), m.seaid@durham.ac.uk (Mohammed Seaid)

1. Introduction

Numerical simulation of wave problems has a vast range of applications in several fields such as acoustics and electromagnetics. However, these applications are severely restricted by the accuracy of the numerical methods used in the modeling. Although, the models can accurately replicate the physics of the wave propagations [1, 2], the uncertainties that are involved in different design parameters can render the models unrealistic. Indeed, numerical simulations can be very convincing to the extent that they may easily mislead the design study. For instance, the iPhone 4 antenna design is a very well known case in this regards, where the uncertainty in the user's grip position caused a major design failure [3]. Therefore, it is of prominent importance to try and evaluate uncertainties in these models. In the current work, we mainly focus on acoustic problems modeled with a deterministic approach namely, the finite element method. The need for Uncertainty Quantification (UQ) in numerical simulations has been highlighted in many studies for different applications such as computational hydraulics [4] and gas dynamics [5] among others. In applied acoustics, the compliance with noise regulations often involves evaluating a range of uncertainties related to the noise source and the conducted measurements [6]. For example, the compliance with a noise criterion in a standard building involves levels that must never be exceeded and levels that can be exceeded for some of the time say 20% of the time. In wave problems, different studies have shown that the uncertainty in computations is mainly due to the inaccurate calibration of wavenumbers [7, 8]. In [9], the authors compute an adjoint model on which it is possible to perform Monte Carlo simulations at a lower computational cost. This method was specifically designed to estimate the risk of instabilities in thermo-acoustic simulations. In order to reduce the computational cost further, some surrogate models were built using few simulations of the adjoint model in [7]. Different approaches were also tested, especially for thermo-acoustic problems ranging from simple linear regression to the more advanced methods including the active subspace method coupled with the linear regression, see [8] among others. Although these works have led to interesting results in the application context, they present two main drawbacks: first adjoint models are needed in their formulations which are very challenging from a computational point of view. Second, these methods are stable for a limited range of uncertainty, compare for example [7] and further reference are therein. Consequently, if the Helmholtz equation is coupled with hydrodynamic models for example, these methods could be of limited use. One way to alleviate these limitations is achieved by using powerful surrogate models that do not need the computation of the adjoint model.

The Polynomial Chaos Expansion (PCE) is very well suited for this class of models with stochastic inputs. The PCE relies on the spectral projection of the model response on a space spanned by an orthogonal polynomial basis with respect to the assumed probability distribution of the uncertain parameter. This surrogate model has been successfully implemented for different applications, see [10, 11, 12] among others. In general, there exist many different ways to develop a PCE for a given problem. The first way consists on computing the polynomial surrogate intrusively for which the whole numerical model needs to be modified, see for example [13, 5]. However, its applicability remains limited due to the fact that the numerical model needs to be modified. On the other hand, non-intrusive methods

to build the PCE also exist. These methods are well known, and have proven the ability to quantify uncertainty accurately even for complex numerical models, see for instance [14]. One of the methods widely used to build the PCE is the regression method which relies on minimizing the square error *i.e.* the square of the distance between the model and the surrogate using the Least-square (LS) method, see for example [15]. These techniques are well suited for problems with high stochastic dimensions (number of uncertain parameters) for which a higher-interpolation level is required to achieve a satisfactory accuracy [16, 17]. Another advantage of these methods is the fact that they can easily be coupled with other methods such as proper orthogonal decomposition (POD) [18], principal component analysis (PCA) [19], and principal generalized decomposition [20] among others. This is especially appealing when the dimension of the model simulation is very large. This has been recently investigated in the context of acoustic waves in [21]. The results reported in this study have shown a great potential of this non-intrusive method to be adopted for modeling stochastic acoustics. However, when the stochastic dimension is not very large, the projection methods are more attracting as very few simulations are enough to correctly build the PCE with a high accuracy. The Non-intrusive Spectral Projection (NISP) method uses the orthogonality propriety of the PCE basis to project the simulation results. This allows one to use some deterministic design of experiment instead of the one based on crude Monte Carlo simulations. This method has been successfully applied to different research areas such as hydraulics [4], aerodynamics [22], and mechanics [23] among others. In the context of acoustic waves, the NISP method has been implemented in many studies. For instance, in [24] the NISP method is used to assess the propagation of uncertainty in coupled hydrodynamic and acoustic models. The NISP has also been applied for the uncertainty quantification of aeroacoustic waves in cavity flows in [25]. In both studies reported in [24, 25], the projection method has allowed to quantify the uncertainty with high accuracy and using few number of simulations compared to the classical methods. In [26], the authors have also demonstrated the convergence of the NISP method applied to acoustic waves with uncertain shape deformations.

It should be stressed that, the deterministic solution for the wave problem requires a considerable simulation time which can be a serious limitation when using standard stochastic methods for the uncertainty quantification. In computational acoustics, often several degrees of freedom are required per-wavelength in order to achieve a meaningful result. As high wavenumbers/frequencies are considered, the number of required degrees of freedom per-wavelength must be increased to retain the same accuracy. This phenomenon is usually referred to as the pollution error and has been investigated in the literature, see for instance [27, 28]. Indeed, due to the pollution error, evaluating one sample at high frequencies can easily become prohibitively demanding in terms of computational costs, not to mention evaluating hundreds or even thousands of samples [29]. To reduce the computational efforts of modeling wave problems at high frequencies, different approaches have been studied in the literature. In general high-order spatial discretizations are more efficient and suffers less pollution, see for example [29]. This is true in the context of the standard finite element methods with high-order polynomials as well as in the context of high order oscillatory functions [30, 31, 32]. However, a main advantage of the oscillatory functions can be achieved by directly injecting them into the approximation without having to change the meshing procedure while high-order polynomials may also require remeshing

with high order elements. Injecting the oscillatory functions into the approximation can be easily achieved using the Partition of Unity Finite Element (PUFE) method [33]. Different types of oscillatory functions were studied for wave problems, see for instance [34, 35]. The method was also implemented for acoustic problems [36, 37, 38, 39], elastic problems [40, 41], and electromagnetic waves [42] as well as for vibro-elasticity [43]. Extension of the method to time-domain applications was investigated in [44, 45] and it was adopted in [46] for solving the inverse problem in acoustics. Oscillatory functions are used to enrich the finite element method using a discontinuous Galerkin formulation or Trefftz-type elements [47, 48]. A comprehensive literature review on Trefftz methods for the Helmholtz equation can be found in [49].

In the present work, we aim to investigate the implementation of the NISP method in the UQ for wave problems at high frequency. We seek to develop a robust method that allows for high accuracy and significantly reduces the computational cost required for the UQ. This goal is achieved by combining the advantages of the NISP method and the partition of unity method. Here, the deterministic simulations are obtained at a low computational cost thanks to the introduction of partition of unity finite element method. The use of polynomial chaos as a surrogate model is motivated by the results of our previous work [21], where we have assessed the quality of the PCE to quantify the uncertainty in acoustic waves using standard finite element methods for plane wave and scattering wave problems at very low frequency. In the present study, the emphasis is on acoustic waves at high frequency for which very fine meshes are required to capture their acoustic features. It is well known that in the case of acoustic waves at high frequency, the conventional finite element methods are computationally very demanding for the deterministic case. The aim of the current study is on the implementation of a class of partition of unity methods for uncertainty quantification in acoustic waves at very high frequency. These problems being already computationally demanding and because only the wavenumber is considered to be stochastic, the sampling strategy could also be improved in order alleviate further the needed number of simulations. For this reason we compare the results computed using the PCE and the standard Monte Carlo method to those obtained using the NISP based on the quadrature method. The results are presented for an interference problem at a square domain and for a scattering wave problem. The combined NISP and partition of unity methods allow to assess the impact of stochastic high wavenumbers on the propagation of uncertainties in the wave problem under study. Numerical results are presented for waves interference in a squared domain and wave scattering by a circular cylinder at high wavenumbers. In order to assess the robustness of the proposed method, comparisons to the full crude Monte Carlo simulations and the regression based PCE are carried out. The present work is among the first to quantify uncertainty in wave problems at high frequencies thanks to the double combined efficiency of NISP and the partition of unity method. The rest of the paper is organized in the following way. In Section 2 we formulate the partition of unity finite element method for acoustic waves. The non-intrusive spectral projection for uncertainty quantification is presented in Section 3. Section 4 is devoted to numerical results for two examples wave problems. Our concluding remarks are given in Section 5.

2. Partition of unity finite element method for acoustic waves

For time-harmonic wave propagation the wave equation can be reduced to the Helmholtz equation which in two-dimension can be written as

$$\Delta u + k^2 u = 0, \qquad \text{in} \quad \mathcal{D}. \tag{1}$$

Here, $\mathcal{D} \subset \mathbb{R}^2$ is the spatial domain, $u(x, y)$ the time-independent wave field at the point $\boldsymbol{x} = (x, y)^\top$, k the wavenumber and Δ the Laplace operator. Although waves can propagate to infinity, it is necessary to truncate the domain at some artificial boundary $\partial\mathcal{D}$ so that the computation can be performed on a finite domain. Furthermore, to avoid introducing errors through this truncation we choose to impose analytical solutions on the boundary $\partial\mathcal{D}$, which is achieved using a mixed boundary condition

$$\frac{\partial u}{\partial \mathbf{n}} + \mathrm{i}ku = g, \qquad \text{on} \quad \partial\mathcal{D}, \tag{2}$$

where $\mathbf{n}$ is a unit normal vector on $\partial\mathcal{D}$, $g(x, y)$ is a source term and i is the unit imaginary number with $\mathrm{i} = \sqrt{-1}$. To solve the boundary value problem defined by (1)-(2) we multiply the Helmholtz equation with a weighting function $v(x, y)$ and integrate over $\mathcal{D}$. Thus, the following weak formulation is obtained

$$\begin{aligned} \int_{\mathcal{D}} \left(\Delta u + k^2 u\right) v \, d\boldsymbol{x} &= 0, \\ \oint_{\partial\mathcal{D}} \left(\frac{\partial u}{\partial \mathbf{n}} + \mathrm{i}ku\right) v \, d\boldsymbol{x} &= \oint_{\partial\mathcal{D}} gv \, d\boldsymbol{x}. \end{aligned} \tag{3}$$

Using integration by parts and substituting the boundary conditions, the weak formulation (3) can be rewritten as

$$\int_{\mathcal{D}} \left(\nabla u \cdot \nabla v - k^2 uv\right) \, d\boldsymbol{x} + \mathrm{i}k \oint_{\partial\mathcal{D}} uv \, d\boldsymbol{x} = \oint_{\partial\mathcal{D}} gv \, d\boldsymbol{x}. \tag{4}$$

To solve this formulation with the finite element method the domain is meshed into a set of N_e conforming, intersecting and not overlapping elements $\mathcal{T}_i$ with $i = 1, 2, \ldots N_e$. We then redefine the computational domain $\mathcal{D}_h \subseteq \mathcal{D}$ to be the union of all these elements. Using the PUFE method, the wave field $u(\boldsymbol{x})$ at any given point can be approximated in term of the nodal values u_i

$$u(\boldsymbol{x}) \approx u_h(\boldsymbol{x}) = \sum_{i=1}^{N_n} \mathcal{N}_i(\mathbf{x}) u_i, \tag{5}$$

where $\mathcal{N}_i(\boldsymbol{x})$ are the conventional polynomial shape functions at a node i and N_n the total number of nodes in the computational domain. Using the partition of unity approach the nodal values are expanded into a linear combination of a sum M of enrichment functions so that the approximation (5) can be rewritten as

$$u_h(\boldsymbol{x}) = \sum_{i=1}^{N_n} \sum_{j=1}^{M} \mathcal{N}_i(\mathbf{x}) \phi_{i,j}(\mathbf{x}) U_{(i-1)M+j}, \tag{6}$$

with $\phi_{i,j}(\boldsymbol{x})$ being the jth order enrichment function at node i and $U_{(i-1)M+j}$ the amplitude of this enrichment function. Similarly, we chose the weighting function $v(x, y)$ to also be formulated in terms of the nodal values V_i as

$$v(\boldsymbol{x}) = \sum_{i=1}^{N_n} \sum_{j=1}^{M} \mathcal{N}_i(\mathbf{x}) \phi_{i,j}(\mathbf{x}) V_{(i-1)M+j}. \tag{7}$$

Usually for wave problems oscillatory functions are chosen for the enrichment which enables approximating the wave field with multi-wavelengths sized elements. In this work we chose a basis of plane waves for the enrichment which is a common choice for Helmholtz problem [34]. To evaluate the integrals in (4) for the oscillatory enrichment functions over such large elements a high-order quadrature scheme is usually needed. Here, all the integrals are evaluated numerically using Gaussian quadrature. The weak formulation then results in the following linear system

$$[\mathbf{K}]\{\mathbf{u}\} = \{\mathbf{f}\}. \tag{8}$$

It should be stressed that the number of degrees of freedom at each mesh node is expanded by the number of enrichment functions M in the partition of unity approximation compared to the conventional finite element methods. However, the total number of degrees of freedom and therefore the size of the linear system (8) in the partition of unity method, remains much smaller than in the standard finite element method thanks to the coarse meshes used for this case. For the computational results presented in this study, the resulting linear systems are solved using an LU decomposition.

3. Non-intrusive spectral projection for uncertainty quantification

In the current work, we are interested in solving stochastic wave problems at high frequency. Therefore, accounting for a stochastic input parameter ζ in the equations(1)-(2), the stochastic Helmholtz problem reads

$$\begin{aligned} \Delta \boldsymbol{U} + k^2 \boldsymbol{U} &= 0, \qquad \text{in} \quad \mathcal{D}, \\ \frac{\partial \boldsymbol{U}}{\partial \mathbf{n}} + \mathrm{i}k\boldsymbol{U} &= \boldsymbol{G}, \qquad \text{on} \quad \partial\mathcal{D}, \end{aligned} \tag{9}$$

where $\boldsymbol{U}(\zeta, x, y)$ is the stochastic wave potential, $k(\zeta)$ the stochastic wavenumber and $\boldsymbol{G}(x, y)$ the boundary function. In this section, we briefly discuss techniques used for polynomial chaos expansions and especially those used to estimate the spectral coefficient. Details on the application of these tools for quantifying uncertainties in waves are also presented here.

3.1. Polynomial chaos expansions

The probabilistic framework is a common approach to propagate uncertainty in the numerical models for many applications in science and engineering. In this case, the uncertain wavenumber parameter should be considered as a random variable. For this purpose, we assume that $(\Omega, \mathcal{F}, \mathcal{P})$ is a probabilistic space where Ω is an event space associated with a σ-algebra $\mathcal{F}$ and a probabilistic measure $\mathcal{P}$. Consequently, we define the random variable as $k(\zeta) : \Omega \longrightarrow \mathcal{R}_i \subset \mathbb{R}$. Moreover, we assume that the random variable $k(\zeta)$ is of finite variance and fully defined by a probabilistic measure. In the present work, this probabilistic measure will be considered as a Normal distribution $\mathcal{N}(\mu_k, \sigma_k)$, where μ_k is the mean value of the wavenumber and σ_k its standard deviation. When solving numerical models subject to uncertain parameters, one can entirely assume that the model response (here the wave field $u(x, y)$)

is viewed as a random field (because the response depends on space) which we denote by $\boldsymbol{U}(\zeta, x, y)$ and it is assumed to be a stochastic process of finite variance. Based on the homogeneous chaos theory, the random field $\boldsymbol{U}(\zeta, x, y)$ can be decomposed into an orthogonal polynomial basis, see [50, 51] among others. In the present work, only the Gaussian measure is considered and the optimal associated basis is identified as the Hermite polynomial basis. This method is well known in the community by Polynomial Chaos Expansion (PCE), see for instance [52, 53]. The PCE has been intensively used as a surrogate model in the context of uncertainty quantification. It aims to reproduce the global behavior of a numerical simulation following a polynomial decomposition. Here, the decomposition of the simulation response $\boldsymbol{U}(\zeta, x, y)$ is given by

$$\boldsymbol{U}(\zeta, x, y) = \sum_{i \in \mathbb{N}} \alpha_i(x, y) \Psi_i \left(k(\zeta)\right), \tag{10}$$

where α_i are the spectral coefficients of the decomposition to be determined and $(\Psi_i)_{i \geq 0}$ are the orthogonal polynomial basis (Hermite polynomials in the present case). In practice, the sum in (10) is truncated to a finite series as

$$\boldsymbol{U}(\zeta, x, y) \approx \sum_{i \in \mathcal{I} \subset \mathbb{N}} \alpha_i(x, y) \Psi_i \left(k(\zeta)\right). \tag{11}$$

where $\mathcal{I}$ is a finite subset of $\mathbb{N}$. Note that the truncation of the polynomial decomposition will surely introduce an error known as the truncation error. Although the Cameron-Martin theorem [54] ensures the ℓ_2 convergence of the equation (10) in the probabilistic sense, the truncation of the equation in the form of (11) will introduce an error which needs to be quantified. Therefore, the determination of a PCE is conditioned by the estimation of the spectral coefficients α_i in (11).

The regression method for the estimation of coefficients is based on solving a Least-Square (LS) minimization problem in the ℓ_2-norm to estimate the coefficients α_i, see for instance [55, 15]. In practice, we begin by defining an error $\{\boldsymbol{\varepsilon}\}$ as the distance between the model and the PCE for a finite set of randomly sampled input variables of size N_{ls} as

$$\boldsymbol{\varepsilon} = \boldsymbol{U}\left(\boldsymbol{\Xi}, x, y\right) - \sum_{i \in \mathbb{N}} \alpha_i(x, y) \Psi\left(k(\boldsymbol{\Xi})\right) \equiv \boldsymbol{\mathcal{U}} - \boldsymbol{\alpha}^\top \boldsymbol{\Psi}, \tag{12}$$

where $\boldsymbol{\Xi} = \left(\boldsymbol{\zeta}_1, \ldots, \boldsymbol{\zeta}_{N_{ls}}\right)^\top$ is the set of N_{ls} realizations for the stochastic input variables $\boldsymbol{\zeta}$ using random number generation and $\boldsymbol{\mathcal{U}} = \left(\boldsymbol{U}_1, \ldots, \boldsymbol{U}_{N_{ls}}\right)^\top$ is the vector of associated model outputs. We also define $\boldsymbol{\alpha} = \left(\alpha_0, \alpha_1, \ldots, \alpha_{N_{PC-1}}\right)^\top$ as the vector of the $N_{PC} = Card(\mathcal{I})$ unknown coefficients and $\boldsymbol{\Psi}$ is the $N_{PC} \times N_{ls}$-valued matrix assembling the values of all orthonormal polynomials at the stochastic input realizations values $\boldsymbol{\Psi}_{ik} = \Psi_i(\boldsymbol{\zeta}_k)$, with $i = 0, 1, \ldots, N_{PC-1}$ and $k = 1, 2, \ldots, N_{ls}$. Hence, the LS method to estimate the set of coefficients $\boldsymbol{\alpha}$ in (12) is equivalent to minimize the following function

$$J(\boldsymbol{\alpha}) = \boldsymbol{\varepsilon}^\top \boldsymbol{\varepsilon} = \left(\boldsymbol{\mathcal{U}} - \boldsymbol{\alpha}^\top \boldsymbol{\Psi}\right)^\top \left(\boldsymbol{\mathcal{U}} - \boldsymbol{\alpha}^\top \boldsymbol{\Psi}\right), \tag{13}$$

and its solution is obtained by solving the following linear system of algebraic equations

$$\boldsymbol{\alpha} = \left(\boldsymbol{\Psi}^\top \boldsymbol{\Psi}\right)^{-1} \boldsymbol{\Psi}^\top \boldsymbol{\mathcal{U}}. \tag{14}$$

It should be stressed that the input space exploration is fulfilled via a Monte Carlo sampling-based approach as discussed in [56, 57] among others.

3.2. Non-intrusive spectral projection

The focus in the present work is on non-intrusive approaches to numerically compute the coefficients $\alpha_i(x, y)$ in (10) using N deterministic simulations. Here, the spectral projection relies on the orthonormality property of the polynomial basis and the ith coefficient $\alpha_i(x, y)$ is computed using the following scalar product

$$\alpha_i(x, y) = \Big\langle \boldsymbol{U}(\zeta, x, y), \Psi_i \Big\rangle = \int_{-\infty}^{\infty} \boldsymbol{U}(\zeta, x, y)\, \Psi_i(\zeta)\, \pi(\zeta)\, d\zeta, \tag{15}$$

where $\pi(\zeta)$ refers to the probability density function of ζ considered to be a Gaussian law in the present work. Consequently, the Gauss-Hermite quadrature rules are used in order to compute numerically the integral term in (15). Following for example [58], one can approximate (15) by

$$\alpha_i(x, y) = \Big\langle \boldsymbol{U}(\zeta, x, y), \Psi_i \Big\rangle \approx \sum_{k=1}^{m} \boldsymbol{U}(\zeta_k, x, y)\, \Psi_i(\zeta_k)\, \omega_k, \tag{16}$$

where the nodes ζ_k are the zeros of the mth-order Hermite polynomial, ω_k are the corresponding weights defined in [59] and $\boldsymbol{U}(\zeta_k, x, y)$ is the deterministic solution computed using a value of ζ_k in the Gauss-Hermite quadrature rule. In (16), m is the number of quadrature roots required in each uncertain direction to ensure an accurate calculation of the integral $\Big\langle \boldsymbol{U}(\zeta, x, y), \Psi_i \Big\rangle$. Indeed, a quadrature rule with m points is exact for polynomials up to the order $(2m - 1)$, see for example [60]. Here, this rule is used in order to define the required number of the simulations when the NISP method is considered. Note that this method has been proven to be very reliable in such cases, especially when the stochastic dimension is not high (less than 5), see for instance [61, 4].

Next, to estimate the statistical moments of the reference solution we use the common method based on stochastic approach using a large sample of simulations. Let N_{mc} denotes the sample size and this sample is generally generated through a standard Monte Carlo (MC) approach based on random variable $k(\zeta)$. The random field representing the stochastic solution can be computed by integrating the forward model such that the equation (9) is solved for each realization value of the parameter in the design of experiment. Hence, the moments of the solution including the mean value $\mu_U(x, y)$ and the standard deviation $\sigma_U(x, y)$ for the forward model can be stochastically estimated by

$$\mu_U(x, y) = \frac{1}{N_{mc}} \sum_{k=1}^{N_{mc}} U(\zeta_k, x, y), \qquad \sigma_U(x, y) = \sqrt{\frac{1}{N_{mc} - 1} \sum_{k=1}^{N_{mc}} \Big(U(\zeta_k, x, y) - \mu_U(x, y)\Big)^2}.$$

It is important to mention that, because of the spatial dependence in the model solution, the mean value and the standard deviation are also presented as mean field and standard deviation field.

One appealing advantage of using the PCE lies on the fact that the statistical moments can be easily derived from the spectral coefficients, see for instance [61, 62]. Indeed, thanks to the orthonormality property of the polynomial

approximation, statistical moments of the wave field are straightforwardly derived from the coefficients as

$$\mu_U(x,y) = \alpha_0(x,y), \qquad \sigma_U(x,y) = \sqrt{\sum_{\substack{i\in\mathcal{I}\\ i\neq 0}} (\alpha_i(x,y))^2}, \tag{17}$$

where $\mathcal{I}$ is the set of the polynomial indices. Note that to measure the extent of variability in a given sample, one may be interested in computing the coefficient of variation (CV), also known as the relative standard deviation and defined as the ratio of the standard deviation $\sigma_U(x,y)$ to the mean $\mu_U(x,y)$. We also consider the root-mean-square-error (RMSE) to assess the quality of the PCE in the present study. The main aim is to assess the PCE using both methods to accurately quantify the uncertainty in waves at high frequency. The RMSE is computed for both the estimator of mean and standard deviation fields as

$$\text{RMSE}(\theta) = \int_{x\in\mathcal{D}_x}\int_{y\in\mathcal{D}_y} \left(\theta^{PC}(x,y) - \theta^{MC}(x,y)\right)^2 dxdy,$$

where θ represents either the mean or variance fields, θ^{PC} is the value of the estimator using the PCE, and θ^{MC} is the value of the estimator using the MC simulations based on a very large sample.

4. Numerical results

To evaluate the performance of the non-intrusive spectral projection for UQ of waves at high frequency we consider two different numerical tests. First an interference of plane waves in a squared domain is considered for evaluating the performance of the method in terms of errors compared to the standard methods. In the second example, a plane wave scattering by a circular cylinder is considered where solutions obtained using the PUFE on coarse meshes are investigated. In both examples, we assess the proposed UQ method for numerous values of the mean wavenumber. All the computations were performed on a cluster machine which allows to run 44 simulations in parallel with an available RAM space of 384 GB. This platform offers also the possibility to use the openturns library for UQ developed in [63] and to couple it with different numerical models. In the subsequent sections, we shall use the terminology MC, LS and NISP to refer to the Monte Carlo method, the PCE built using the Least square method and the PCE built Non-Intrusive Spectral Projection method, respectively. In addition, the deterministic solutions are computed using the mean value of the wavenumber.

4.1. Interference of plane waves in a squared domain

In this example, we recover the interference of two plane waves. We solve the Helmholtz problem (1)-(2) in the squared domain $\mathcal{D} = [1,2]\times[1,2]$ where the analytical deterministic solution is given by

$$u(x,y) = e^{\mathrm{i}k(x\cos(\alpha)+y\sin(\alpha))} + e^{\mathrm{i}k(x\cos(2\alpha)+y\sin(2\alpha))}. \tag{18}$$

with α being the wave direction. The analytical solution is imposed on the boundary $\partial\mathcal{D}$ through the source function g in (2). For this problem, the wavenumber k is assumed to be the stochastic parameter defined as

$$k(\zeta_k) = \overline{k}\,(1 + CV\zeta_k)\,, \tag{19}$$

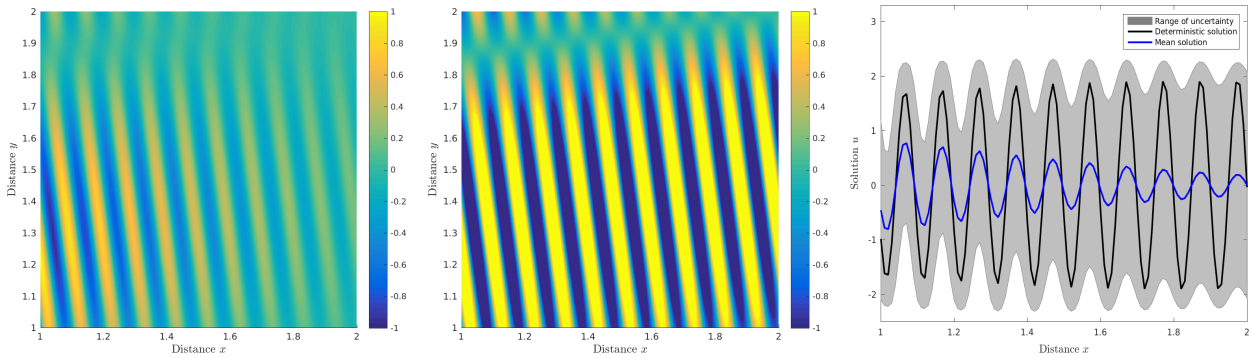

Figure 1: Mean wave potential $\overline{U}(x, y, \zeta_k)$ obtained for the stochastic simulation (first column), the deterministic solution $U(x, y, \bar{\zeta})$ computed using the mean value of k (second column) and a cross-section of the solutions at $y = 1.8$ (third column) obtained for the interference of plane waves problem using $\overline{k} = 20\pi$ and $CV = 10$ %.

where CV is the coefficient of variation associated to the physical deterministic values of the wavenumber $k(\zeta_k)$ and $\overline{k}$ is the mean value of k. In (19), ζ_k are the corresponding random variables which are supposed to follow the centered normal law $\mathcal{N}(0, 1)$. In the results presented for this test example two high values of the mean wavenumber $\overline{k}$ are selected namely $\overline{k} = 20\pi$ and $\overline{k} = 40\pi$. For the partition of unity, we use a uniform finite element mesh composed of 25 square 4-nodded elements where the total number of nodes is 36. The same mesh is retained for both considered wavenumbers but the number of enrichment functions is increased from 28 to 48 plane waves for the higher wavenumber. A fixed value of $\alpha = 5°$ is considered in the simulations. Note that the uncertainty in this example is assessed for the quantities of interest over the acoustic potential $u(\zeta_k, x, y)$.

First, we perform the UQ over the wave problem with a mean wavenumber value set to $\overline{k} = 20\pi$. The uncertainty is propagated in the model induced by stochastic wavenumber using (19). Consequently, we assume that the uncertain parameter follow a Normal distribution $\mathcal{N}(\overline{k}, \sigma_k)$, where $\overline{k}$ is the mean value of the wavenumber that is set to 20π and σ_k refers to the standard deviation. The uncertainty supposed on the wavenumber value is set to $CV_k = 10\%$ which yields $\sigma_k = CV_k \times \overline{k} = 2\pi$. It should be noted that, in subsurface imaging the uncertainty in the wavenumbers can be relatively large mainly due to the uncertainties in the material properties as well as in the subsurface structure. For example, in engineering geology the ground behavior is assumed based on limited information. Therefore, it is a common practice to estimate the likelihood of the subsurface properties so that the impact of this uncertainty can be evaluated from a considered engineering application [64, 65]. In the crude MC simulations, we randomly sample N values $(k_1, \ldots, k_N)$ of k with respect to the distribution $\mathcal{N}(\overline{k}, \sigma_k)$, then for each value a corresponding simulation is performed. Finally a set of N solutions $U = (U_1, \ldots, U_N)$ is obtained corresponding to these N samples. To ensure statistical convergence of the MC method we use a large number of samples $N = 100000$. Here, the deterministic solution $U_{\overline{k}(x,y)}$ obtained using the mean value $\overline{k}$ and the mean solution $\overline{U}_k(x, y)$ are used for comparison. The range of uncertainty is also given by the interval $\left[\overline{U}_k(x, y) - 1.5\sigma_U, \overline{U}_k(x, y) + 1.5\sigma_U\right]$, where σ_U is the standard deviation of the wave potential field.

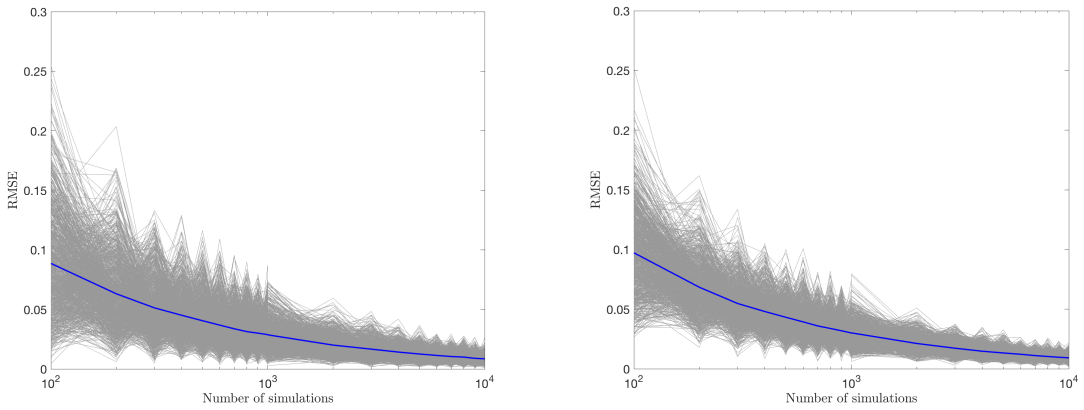

Figure 2: Assessment of the Monte Carlo simulation for the estimation of the mean and the variance fields using a Bootstrap method compared to an expensive Monte Carlo simulation (with 100000 forward simulations).

Figure 1 presents a comparison between the deterministic field and the stochastic mean field. In this figure, we also include cross-sections of the obtained solutions at $y = 1.8$ along with the envelope for the range of uncertainties. It should be mentioned that because of the high stochasticity in this problem, the uncertain envelope is constructed of 1.5 times the standard deviation. Generally, this envelope is chosen according to the engineering problem under consideration. Compared to the deterministic case, it is clear that the stochasticity has an effect of damping on the mean wave field. As can be seen from the cross-sections in Figure 1, the wave amplitude obtained for stochastic simulations decreases along the wave direction and the variance which is translated by the range of uncertainty has a very high value. It should also be noted that the spatial mean value for the coefficient of variation for the field is $CV_U = 412\%$ which is a very high value for little perturbation introduced in the problem. Recall that the coefficient of variation of the wavenumber for this case is set to 10%. From a numerical point of view, building a surrogate model may be very challenging under such conditions, especially for those relying on random number generations as the required number of model evaluations would depend on the variance of the integrand and for some specific designs of experiment on the dimensionality, we refer the reader to [66] for more details. Needless to mention the difficulties related to the approximation of the surrogate model, see the discussions reported in [67, 68] among others.

Next, before the assessment of the suggested meta-model to quantify the uncertainty, the Monte Carlo skills are first evaluated. From a numerical view point, the Monte Carlo simulations are very easy to implement as they require only sampling the stochastic space into a set of random variables. The other major advantage of the method is that, following the Central Limit Theorem [69], the result obtained using the Monte Carlo simulation converges to the true statistical value in the probability sense. This means that each statistical estimation should be addressed within a confidence interval [66]. In practice, it is very hard to obtain the upper and lower bounds of the statistical estimation. In [70], the author introduced the bootstrap method in order to evaluate the probabilities of the Monte Carlo simulation errors. This method consists of rerunning several times the Monte Carlo simulation, the confidence interval could be

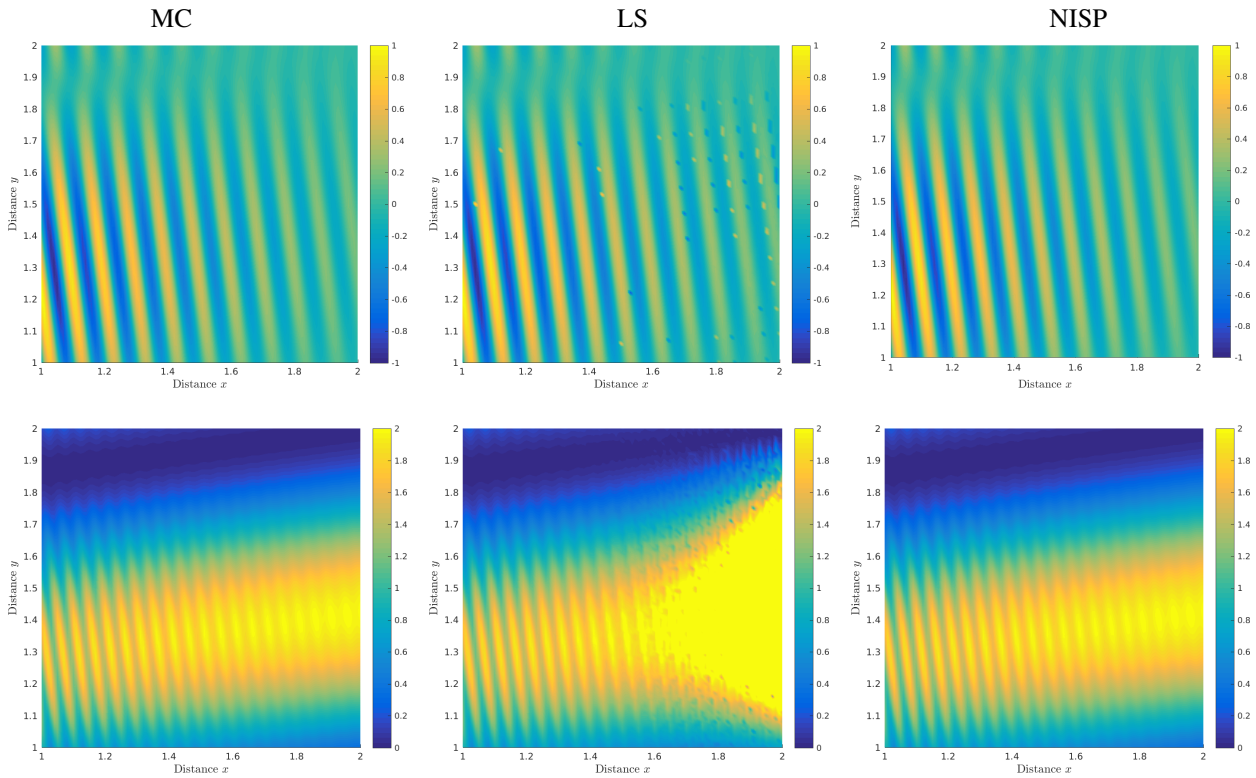

Figure 3: Mean wave potential (first row) and variance solution (second row) computed using the MC simulations (first column), the LS method (second column) and the NISP method (third column) obtained for the interference of plane waves problem in a squared domain using $\overline{k} = 20\pi$.

estimated then for the numerous evaluations of the method. In the present study we use a bootstrap method in order to evaluate the required number of the forward model evaluations to have reliable statistical information. Figure 2 exhibits the results obtained using the bootstrap method for which every statistical information is compared to those obtained with an expensive Monte Carlo simulation containing a hundred of thousand members. It is clear that the Monte Carlo simulation depicts a high level of volatility for the RMSE for the estimation of the mean and the variance fields. The high level of uncertainty displayed in the model increases the required number of simulations which could be predictable. Indeed, for a high precision of the statistical estimation the required number of simulations depends on the variance of the function, we refer the reader to the discussion in [66] for further information. Based on the results obtained by the bootstrap method, one should consider a Monte Carlo simulation with more than ten thousand simulations in order to achieve a reliable statistical estimation. The present results imply also that surrogate models using methods that are based on the random number generation such as the LS would more likely fail compared to the spectral methods because of this large volatility displayed by the Monte Carlo simulation. In addition, as reported in [66] when using the Monte Carlo or quasi-Monte Carlo methods, the statistical estimations are bounded in confidence interval. This interval depends on the variance of the model and therefore when the variance is high (*i.e.* the uncertainty is high) this class of methods is more likely to fail compared to the spectral methods.

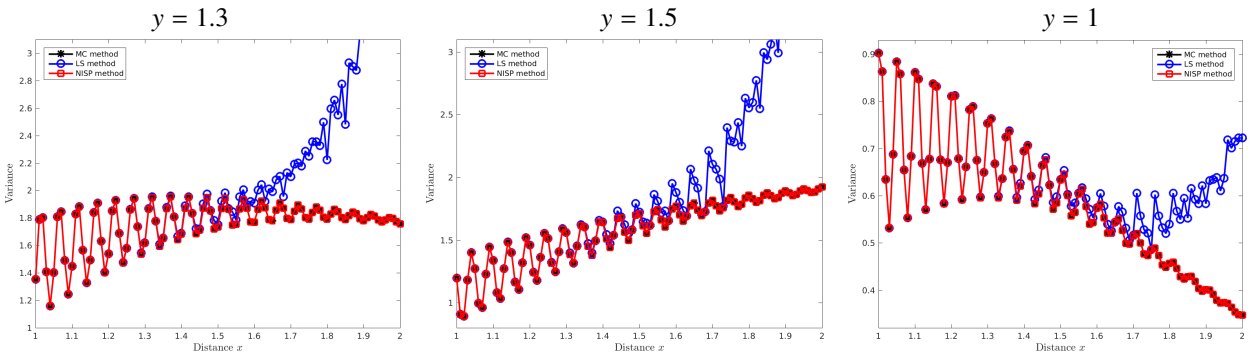

Figure 4: Cross-sections of the variance field at different locations obtained by the three considered methods for the interference of plane waves problem in a squared domain using $\overline{k} = 20\pi$.

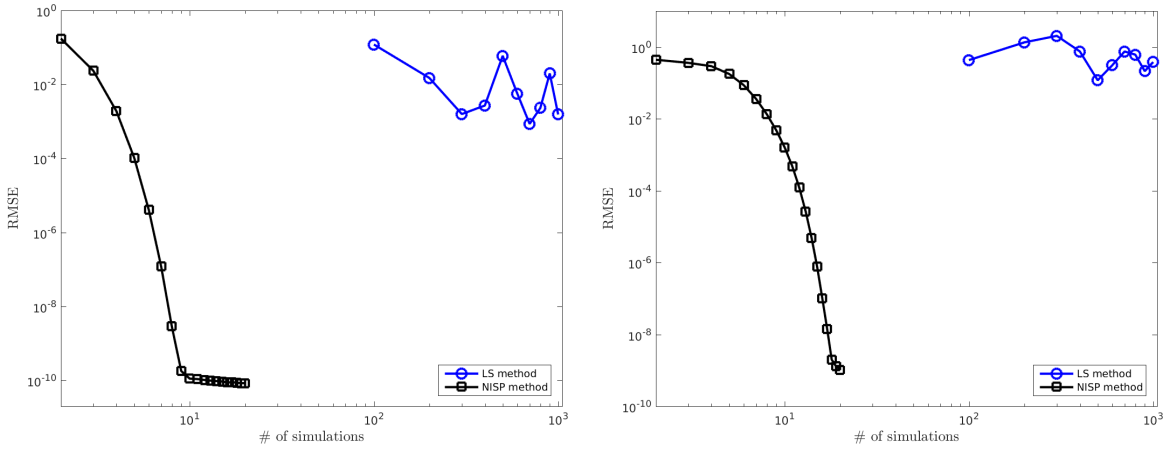

Figure 5: RMSE for the mean wave potential (left plot) and variance solution (right plot) obtained by the MC simulations, LS method and NISP method for the the interference of plane waves problem in a squared domain using $\overline{k} = 20\pi$.

Next, we assess the performance of the PCE in the UQ context using both regression and projection methods. The MC simulations are used as baseline to compute the ℓ_2-error for the surrogate model. Figure 3 compares the spatial mean and variance fields obtained using the three considered methods namely, the MC simulations, the LS based method to build the PCE, and the NISP method to build the PCE. It is clear that for the considered wave conditions the projection method outperforms the regression based method. The spatial mean field is clearly approximated by both methods with a good accuracy. However, the variance field is obviously not well represented by the LS method. Figure 4 depicts horizontal cross-sections of the variance field at different locations. It is clear that in some locations, both LS and NISP methods perform equally well compared to the field obtained using the MC simulations. However, at the same locations, the LS method is struggling to correctly capture the variance field as estimated by the full MC simulations using the large sample. As it can be seen in the spatial variance field, the regression method is particularly noneffective in locations where the wave is rapidly varying along the space.

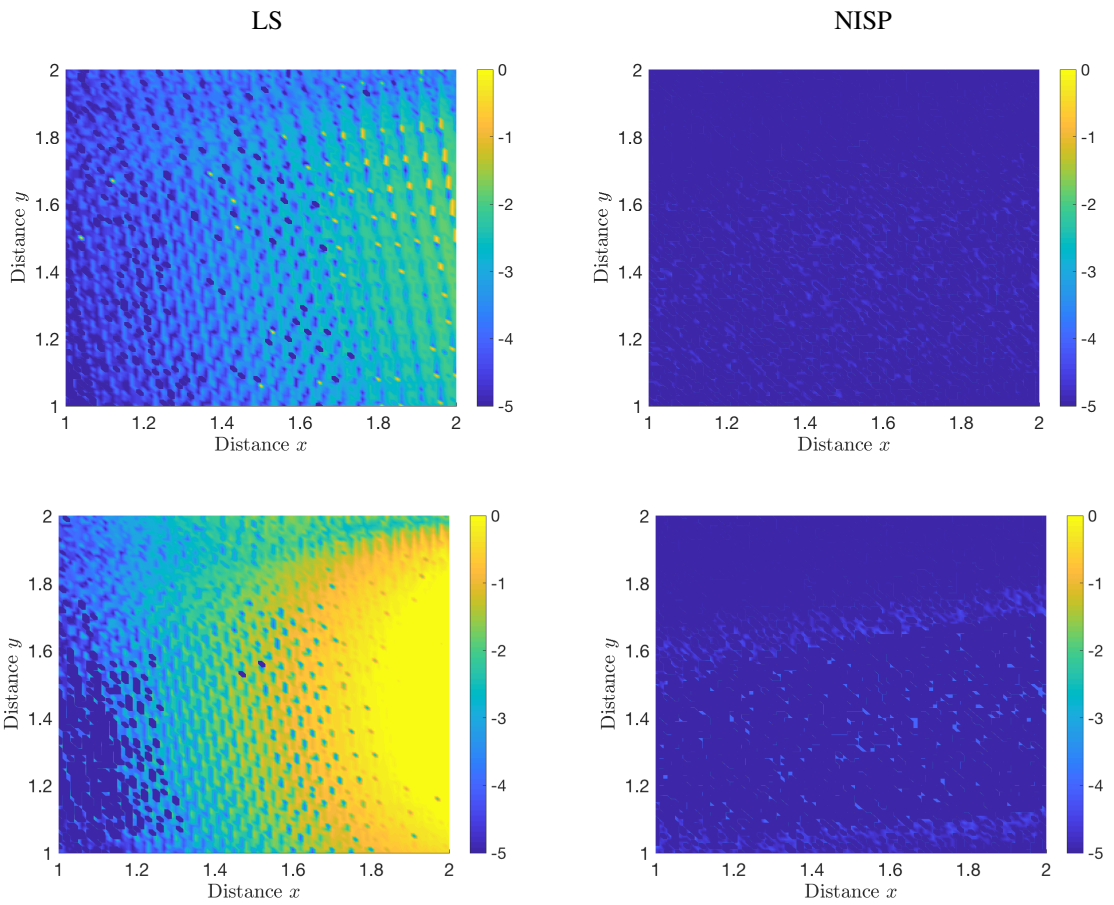

Figure 6: Absolute Error in logarithmic scale for the estimation of the mean (top) and the variance (bottom) using both methods LS (left) and NISP (right) with comparison to MC simulation for the interference problem of plane waves problem in a squared domain using $\bar{k} = 20\pi$.

Table 1: Computational times obtained using the MC simulations, LS method and NISP method for the interference of plane waves problem in a squared domain using $\bar{k} = 20\pi$.

	MC simulations	LS method	NISP method
Number of simulations	100000	1000	9
CPU time (in minutes)	798	12	2

To quantify the results for this test example we compare the RMSE obtained for the mean and variance solutions using the considered methods. Note that, when the PCE is achieved, the mean and variance fields can be analytically derived from the PCE coefficients which is considered to be the main advantage of using a surrogate model based on a spectral method such as the PCE. In Figure 5 we display the evolution of RMSE for different numbers of simulations. This number represents the size of the design for the experiment used to build the PCE. One can see that for both

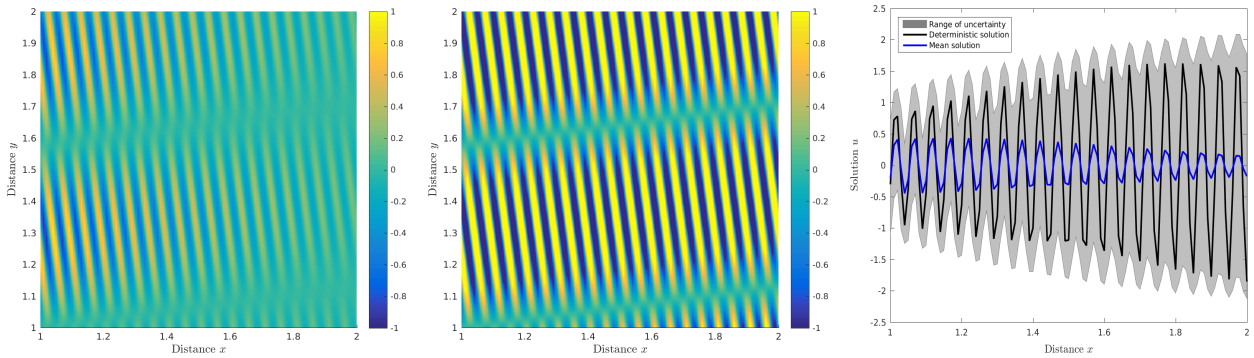

Figure 7: Mean wave potential $\overline{U}(x, y, \zeta_k)$ obtained for the stochastic simulation (first column), the deterministic solution $U(x, y, \bar{\zeta})$ computed using the mean value of k (second column) and a cross-section of the solutions at $y = 1.8$ (third column) obtained for the interference of plane waves problem in a squared domain using $\overline{k} = 40\pi$ and $CV = 10$ %.

estimators the RMSE decreases more rapidly for the NISP than for the regression method. In addition, the RMSE for the mean estimator is always lower than the variance estimator for the considered methods. This is due to the fact the mean requires only the first coefficient of the decomposition which can easily be obtained with few forward simulations whereas, the variance field requires the whole set of coefficients existing in the decomposition. In the case of the regression method, the RMSE for the variance estimator does not decrease less than 10^{-1}. On the contrary, few simulations of the forward model (less than a dozen) are sufficient to build a surrogate model which is able to quantify the uncertainty with a high level of accuracy in the estimation of the statistical moments (with RMSE = 10^{-4} for the estimation of the standard deviation and 10^{-7} for the estimation of the mean). This is also confirmed by results shown in Figure 6 where the absolute error is plotted for the estimation of both statistical moments, namely the mean and the variance using the most converged surrogate model according to its RMSE value. The NISP has a good estimation of both moments fields in all the spatial domain, while the LS methods may have some wrong estimations in some locations.

To further quantify the results for this example we summarize in Table 1 the computational cost (CPU time) required to achieve the best value of the RMSE. Here, the NISP method needs only 2 minutes while the LS method uses 12 minutes and the MC simulations need 798 minutes for the considered 100000 samples. It is evident that the NISP method performs better than the regression based method as it require less number of simulations for more accurate results compared to the MC method. Indeed, the NISP method performs better than the regression method requiring 6 times less CPU time. In comparison with the crude MC simulations, the CPU time is 399 times higher than the NISP method. For this wave problem with $\overline{k} = 20\pi$, the NSIP method is demonstrated to be very robust as it requires significantly less CPU time to perform the UQ with very high accuracy.

In our second run for this problem we aim to assess the robustness of the suggested methods with the mean wavenumber $\overline{k} = 40\pi$. For this situation, the standard finite element method requires a considerable amount of CPU times and the use of the partition of unity in the present study would overcome this drawback and solves this problem

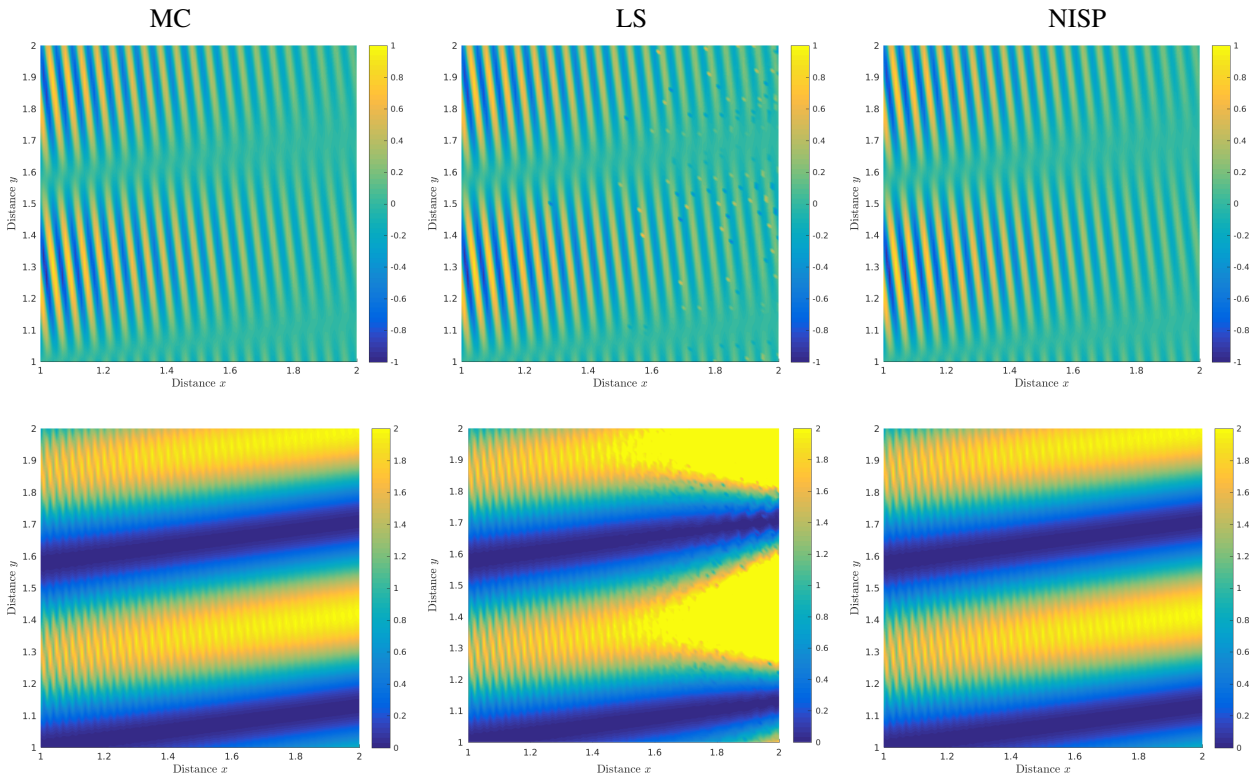

Figure 8: Mean wave potential (first row) and variance solution (second row) computed using the MC simulations (first column), the LS method (second column) and the NISP method (third column) obtained for the interference of plane waves in a squared domain using $\bar{k} = 40\pi$.

at a reasonable computational cost. As for the previous case, we begin first by assessing the uncertainty using the MC method using a large set of forward simulations. Here, the number of simulations used in the MC method is set to 100000 realizations. Note that for this numerical setting, the error in the deterministic simulations is kept less than 0.1%. The considered coefficient of variation on the uncertain wavenumber is set at $CV = 10\%$ *i.e.*, the wavenumber k follows a Normal distribution $\mathcal{N}(40\pi, 4\pi)$.

A comparison between the deterministic and stochastic solutions for this test case is presented in Figure 7. This figure includes also cross-sections of the obtained solutions at $y = 1.8$ along with the envelope for the range of uncertainties. Again, the obtained results show that the uncertainty on the wavenumber translates into damping effects in the wave solution. Moreover, the uncertainty propagated in the numerical model indicates that the stochasticity in the wavenumber results into a considerable range of uncertainty on the wave field. Indeed, for the considered wavenumber, the spatial mean coefficient of variation is estimated over the wave field at 266%. Thus, this case highlights a large amount of uncertainty from the propagation of stochasticity in the wavenumber. Under these circumstances, developing a surrogate model for this test case may be very challenging as discussed above.

In Figure 8 we present comparisons between the mean wave potential and variance solutions computed using the MC, LS and NISP methods. Notice that the MC simulations are assumed to be the most accurate method but at

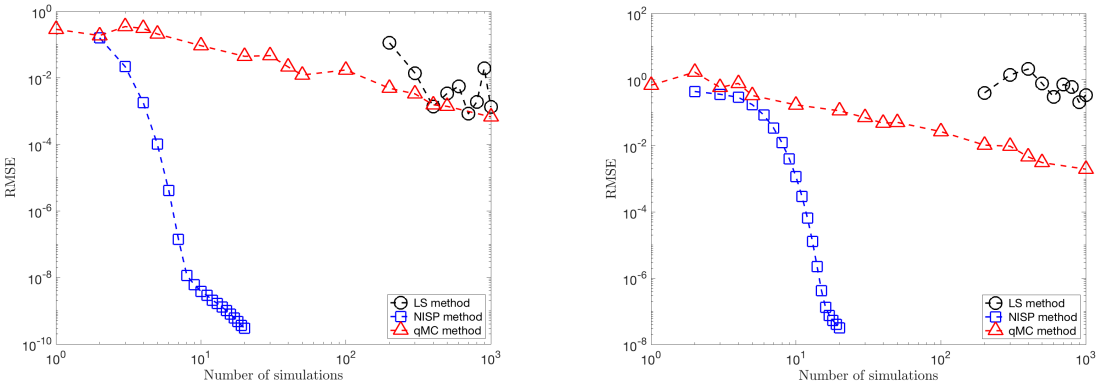

Figure 9: The RMSE for the mean wave potential (left plot) and variance solution (right plot) obtained by the quasi-Monte Carlo simulations, LS method and NISP method for the interference of plane waves problem in a squared domain using $\overline{k} = 40\pi$.

Table 2: Computational times obtained using the MC simulations, LS method and NISP method for the interference of plane waves problem in a squared domain using $\overline{k} = 40\pi$.

	MC simulations	LS method	NISP method
Number of simulations	100000	1000	9
CPU time (in minutes)	886	14	3

high computational cost. In this case, although the three methods agree well on the estimation of the mean field of the wave solution, the LS based method fails to fully converge towards the true variance field as estimated by the fully converged MC simulations. As pointed out previously, the variance field displays some high values with similar spatial features as in the first case with $\overline{k} = 20\pi$. It is also clear that the variance follows the physical spatial field of the wave. Due to the complexity of the wave features in this case, the *butterfly effect* of the uncertain wavenumber is the main reasons of the difficulties in developing surrogate models for waves at high frequency. Furthermore, we compare the results obtained using the quasi-Monte Carlo simulations for this test example. Notice that this class of methods was shown to be useful in reducing the computational burden of uncertainty quantification methods, see for example [71]. These techniques rely on the quasi random number generation for sampling schemes following the Sobol' sequences [72] or the Halton sequences [73] among others. They are very powerful particularly when the stochastic dimension is not high because they are obtained with low discrepancy. Consequently, they are highly dependent on the stochastic dimension as opposed to the standard Monte Carlo simulations. In the present case, we compare the performance of this class of methods to the method proposed in this study. As can be anticipated, the quasi-Monte Carlo simulation performs better than the LS method while, the NISP still performs better. In fact, for the specific case when the stochastic dimension is low, the spectral methods have been demonstrated to be very

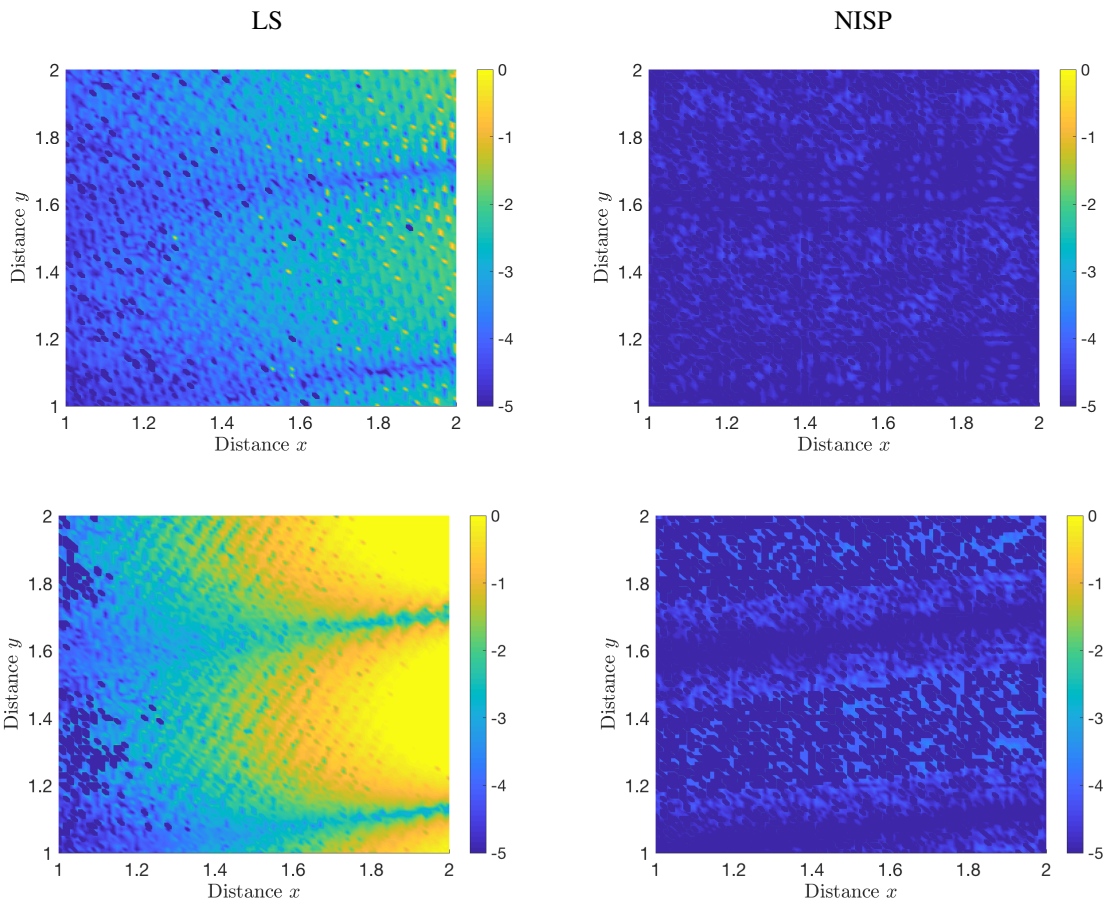

Figure 10: Absolute Error in logarithmic scale for the estimation of the mean (top) and the variance (bottom) using both methods LS (left) and NISP (right) with comparison to MC simulation for the interference problem of plane waves problem in a squared domain using $\bar{k} = 40\pi$.

accurate as a few numbers of simulations is necessary to quantify the uncertainty properly, see for example [14, 61]. As opposed to the quasi-Monte Carlo simulations which are stable and accurate under some conditions on the required number of simulations as discussed in [74] among others. In addition, we assessed the dependency space of the error. For this purpose, Figure 10 depicts the absolute error for the estimation of both statistical moments, namely the mean and variance solutions using the most converged surrogate model according to its RMSE value. Again, the NISP has a good estimation of both moment fields in all the spatial domain, whereas the LS method produced poor local estimates.

For the considered wave conditions, the NISP method seems to accurately perform the UQ with a considerable saving in the CPU time compared to the MC and LS methods, compare Table 2. In this table, we summarize the CPU times required to achieve the best value of the RMSE in the considered methods. It is also clear that the projection method is 295 time less demanding than the converged MC simulations in terms of the computational cost. Compared to the regression method which we recall here is not fully converged, the NISP method requires a CPU time four times

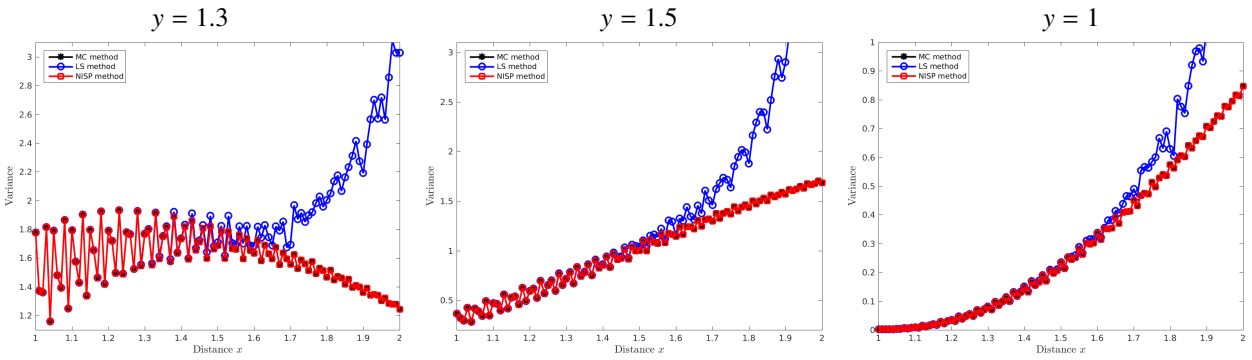

Figure 11: Cross-sections of the variance field at different locations obtained by the three considered methods for the interference of plane waves problem in a squared domain using $\overline{k} = 40\pi$.

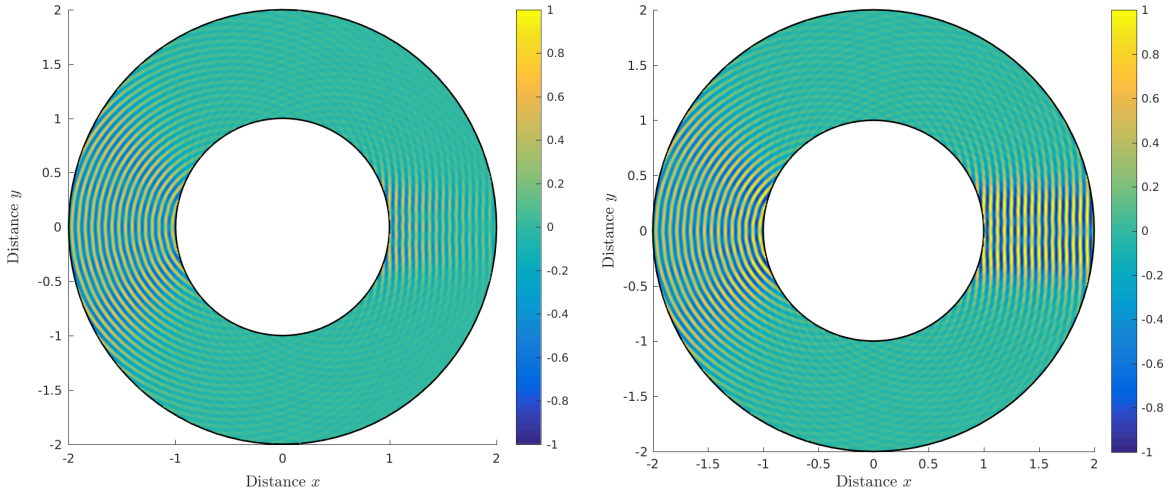

Figure 12: Mean wave potential $\overline{U}(x, y, \zeta_k)$ obtained for the stochastic simulation (left plot), the deterministic exact solution $U(x, y, \bar{\zeta})$ computed using the mean value of k (right plot) obtained for scattering wave by a circular cylinder using $\overline{k} = 32\pi$ and $CV = 10\ \%$.

less. As reported in Figure 9, the NISP method achieved high accuracy faster than the regression based method. It should be stressed that when it converges, the quadrature based method achieves a RMSE estimated at 10^{-5} for the standard deviation and 10^{-8} for the mean solution. This can also be seen in Figure 11 where vertical and horizontal cross-sections of the variance field are illustrated at different locations. It is clear that the regression method fails to be accurate when the variance has high values. In addition, when the uncertainty increases and being a method relying on a LS method, the surrogate model needs more work. This means that the convergence of the regression based method needs more samples which yields a substantial increase in the computational cost.

4.2. Plane wave scattering by a circular cylinder

In this test example we consider the problem of a plane wave scattering by a circular cylinder widely used in the literature to examine the performance of numerical methods for wave problems, see for example [46, 29]. Assuming

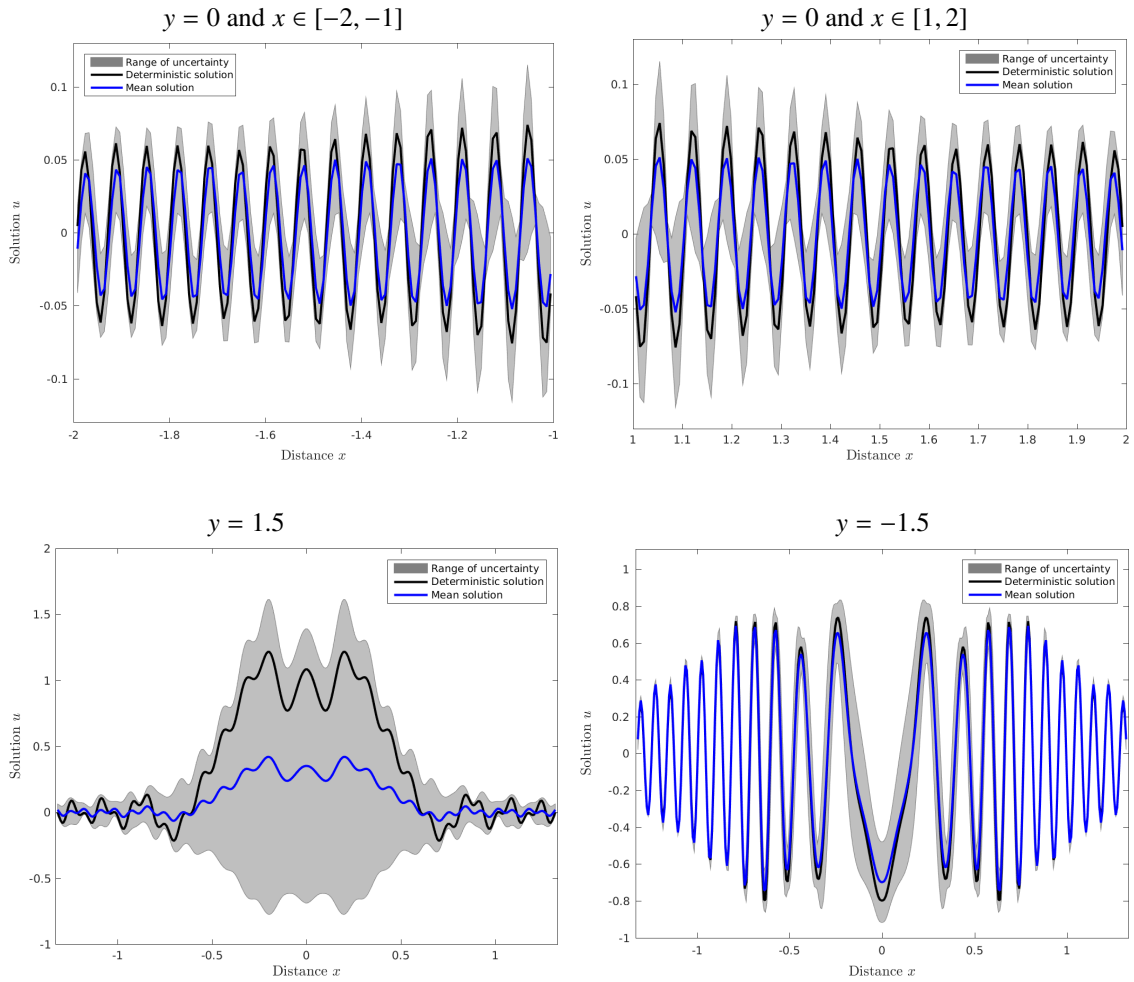

Figure 13: Vertical cross-sections (first row) and horizontal cross-sections (second row) of the mean and the deterministic solutions obtained for scattering wave by a circular cylinder using $\bar{k} = 32\pi$.

that the incident wave propagates in the negative x-axis direction, the scattered wave field can be evaluated analytically as

$$u = -\sum_{n=0}^{\infty} \mathrm{i}\epsilon_n \frac{J_n'(ka)}{H_n'(ka)} H_n(kr)\cos(n\theta), \tag{20}$$

where $\epsilon_0 = 1$, $\epsilon_n = 2$ for $n \neq 0$ and $J_n(ka)$ is the well-established Bessel and $H_n(ka)$ is Hankel function of the first kind and order n. The prime denotes the derivative of a function with respect to its argument. Note that the expression (18) is written in polar coordinate r and θ whereas, the scatter radius is a. The computational domain $\mathcal{D}$ for this example is a ring defined with the inner and outer radii $R_i = 1$ and $R_o = 2$, respectively. The analytical function (20) of the scattered wave is imposed on the domain inner and outer boundaries using Robin-type boundary condition (2). The objective of this test example is to examine the performance of the considered methods for the UQ to resolve the pressure of a plane wave scattered by an infinitely rigid circular scatterer subject to stochastic wavenumbers. In our

Table 3: Computational times obtained using the MC simulations, LS method and NISP method for the scattering wave by a circular cylinder using $\overline{k} = 32\pi$ and $CV = 10$ %.

	MC simulations	LS method	NISP method
Number of simulations	100000	10000	7
CPU time (in minutes)	15541	1063	20

simulations, the wavenumber is considered to be stochastic with a mean value $\overline{k} = 32\pi$ and coefficient of variation $CV = 10$ % around the mean. Thus, the wavenumber follows a Normal distribution $\mathcal{N}(32\pi, 3.2\pi)$. We also use a finite element mesh formed of 4-noded bilinear elements with a total number of 200 elements and 240 nodes. A total of 50 enrichment functions are used in the partition of unity.

We also assess the MC simulations for this wave problem using a full set of 100000 realizations as a baseline for the UQ. Figure 12 illustrates a comparison between the deterministic and the stochastic mean solution fields. For a better insight, vertical and horizontal cross-sections are displayed in Figure 13. Compared to the previous example of plane wave scattering in the squared domain, the damping effects is less pronounced for this test example. Furthermore, the *butterfly effect* is still present in these simulations but it has been relatively diminished. For instance, the spatial mean value for the coefficient of variation in this case is estimated at 93.5 %. These effects can clearly be notable in the cross-sections shown in Figure 13. It should also be pointed out that despite the fact that the uncertainty has diminished in this problem compared to the previous case, development of the surrogate model is still challenging with this level of uncertainty.

Next, we turn our attention to a comparison study of the three considered methods in order to estimate the uncertainty in this scattering wave problem. In Figure 14 we present the stochastic mean and variance fields obtained using the LS based method, the NISP method and the MC simulations. It is clear that for the considered wave conditions, the differences between the results obtained using the three methods are slightly appreciable. For instance, the mean field is well reconstructed using both LS and NISP methods. However, the variance field is better reconstructed using the NISP method than the LS based method. For comparison reasons, cross-sections of the variance field at different locations are reported in Figure 15. At the location close to the scatter, the obtained results using the three methods overlap and at the location far from the scatter, the regression method is less effective.

Finally, we compare the computational cost and the necessary number of simulations needed for each method to achieve the stochastic convergence with respect to the MC simulations baseline. Figure 16 depicts the results of the evolution of RMSE as a function of the necessary number of simulations needed for convergence. The performance of the most converged surrogate model for both LS method and NISP method are compared using absolute error in Figure 17. Note that while the difference is not clear for the mean field unsurprisingly, the NISP method performs

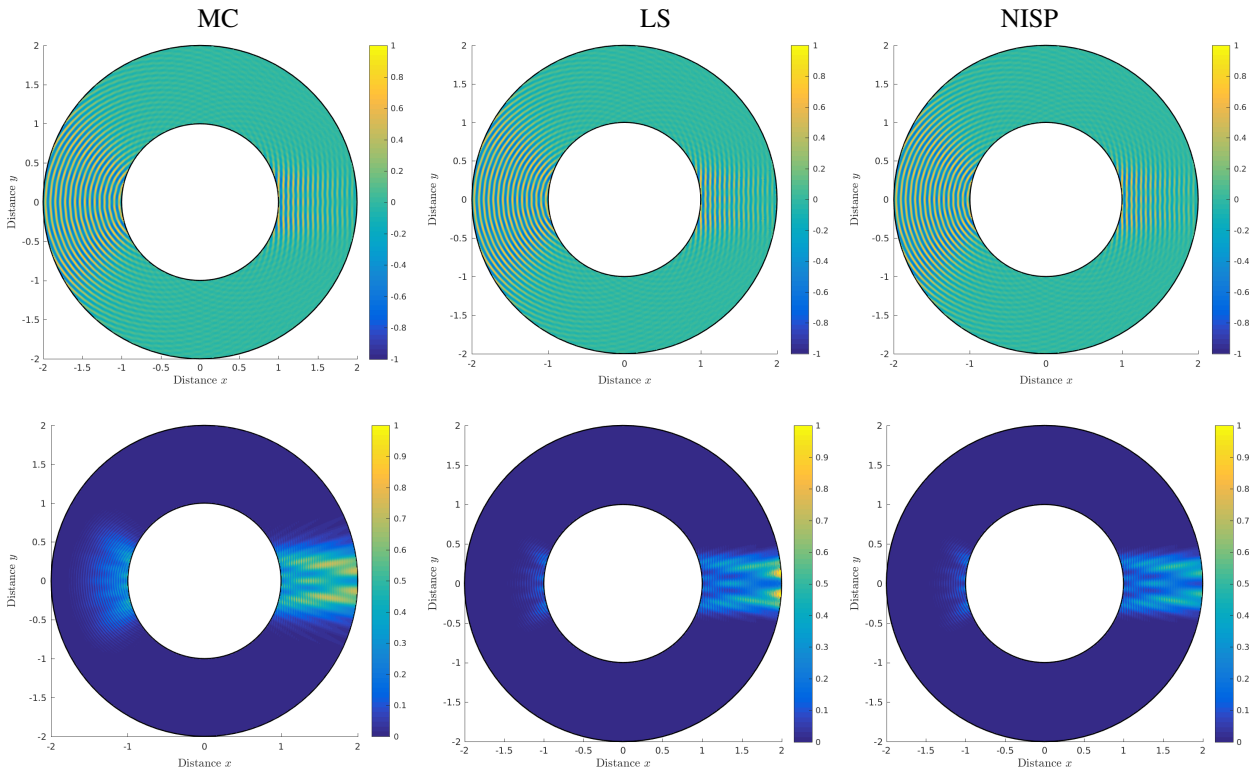

Figure 14: Mean wave potential (first row) and variance solution (second row) computed using the MC simulations (first column), the LS method (second column) and the NISP method (third column) obtained for the scattering wave by a circular cylinder using $\overline{k} = 32\pi$ and $CV = 10$ %.

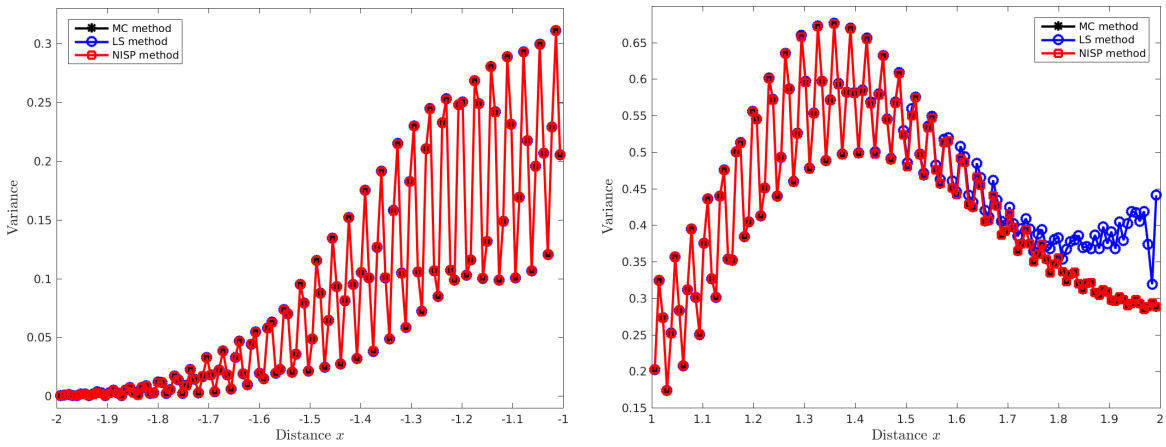

Figure 15: Vertical cross-sections at $x = 0$, $y \in [-2, -1]$ (left plot) and at $x = 0$, $y \in [1, 2]$ (right plot) of the variance fields obtained for scattering wave by a circular cylinder using $\overline{k} = 32\pi$.

better in the estimation of the variance field. To further quantify the results for this example we summarize in Table 3 the computational cost (CPU time) required to achieve the best value of the RMSE. As for the previous case, the

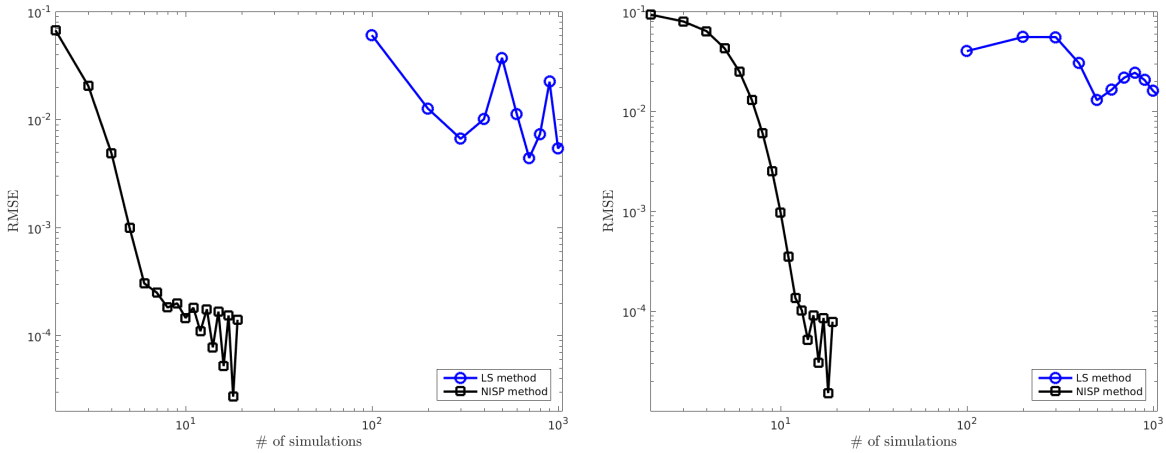

Figure 16: The RMSE for the mean wave potential (left plot) and variance solution (right plot) obtained using the MC simulations, LS method and NISP method for the scattering wave by a circular cylinder using $\overline{k} = 32\pi$.

NISP method allows to achieve a good accuracy more rapid than the LS method. For this test example, 7 simulations in the NISP method perform better than the regression based method with 10000 simulations. In comparison with the crude MC simulations, the CPU time is 777 times higher than the NISP method. For this scattering wave problem with $\overline{k} = 32\pi$, the NSIP method is demonstrated to be very robust as it requires few CPU times to perform the UQ with very high accuracy.

5. Conclusions

In the present study we have performed the uncertainty quantification for wave problems at high frequency. The uncertainty is assumed to be resulting from high values of wavenumbers in the problems under study. Solving such problems using finite element methods is very challenging. The literature shows that using an enriched finite element approach can significantly reduce the computational costs of solving forward wave problems. Here, we have used plane waves as enrichment functions in the partition of unity approximation. In the current work, we have evaluated the use of polynomial chaos expansion in a non-intrusive manner. This method relies on the Galerkin projection using a deterministic design of experiment. Numerical results are presented for two sets of numerical experiments, first for interference of waves and then for a wave scattering by a circular cylinder at high wavenumbers. Both sets are considered at high frequencies and evaluated using a regression based method and the non-intrusive spectral projection. The uncertainty quantification is achieved by combining the advantages of both the non-intrusive techniques and the partition of unity finite element discretizations. The proposed approach has led to a major reduction in the time required to perform the computations by several orders of magnitude without compromising the accuracy. It should be stressed that comparisons of the CPU time do not include the cases where the forward problem is solved with the standard finite element method where in this case the simulations would have become practically lengthy.

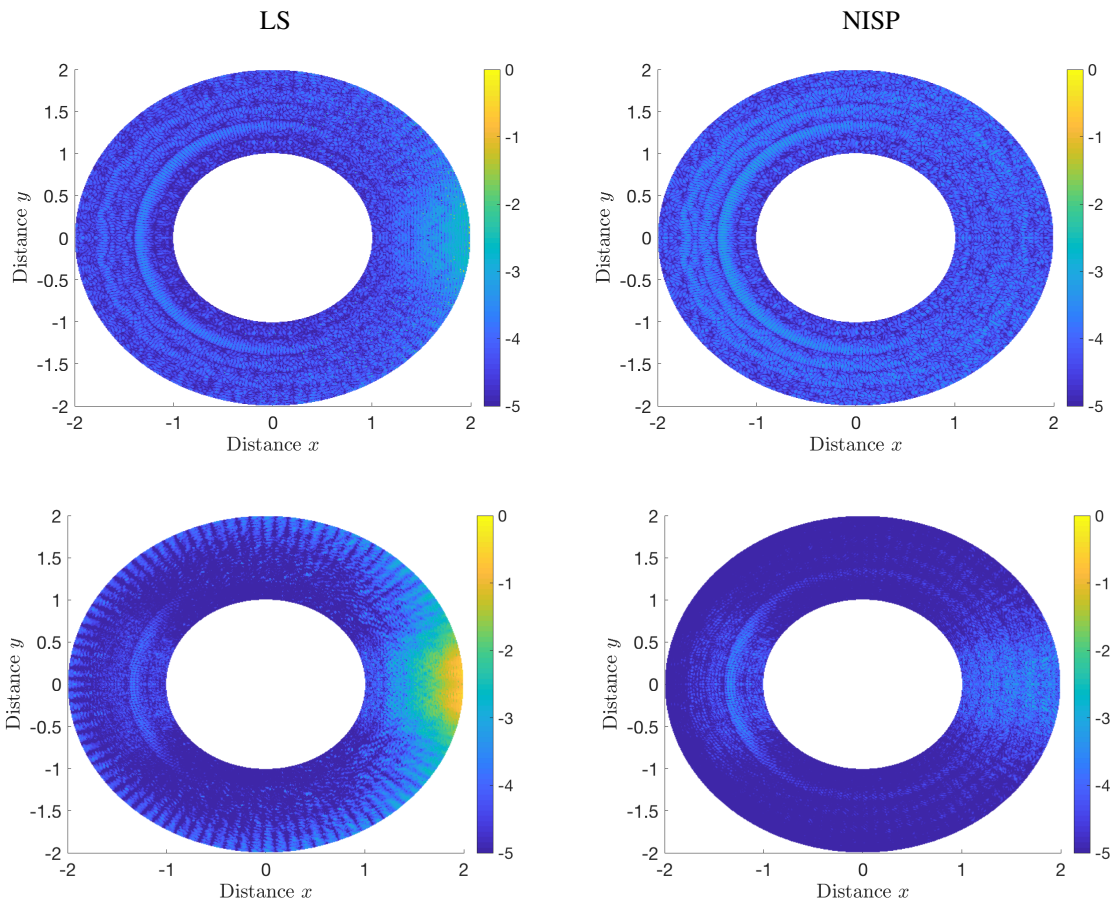

Figure 17: Absolute Error in logarithmic scale for the estimation of the mean (top) and the variance (bottom) using both methods LS (left) and NISP (right) with comparison to MC simulation obtained for scattering wave by a circular cylinder using $\bar{k} = 32\pi$.

Comparisons to the well-established Monte Carlo simulations have been presented for the interference of plane waves in a squared domain and a scattering wave problem. The computed results demonstrate that accounting for the propagation of the uncertainty in the wavenumber through the model, the wave solution exhibits a large amount of uncertainty. In the scattering wave problem we have also highlighted an increase in the uncertainty for areas located far from the scatter. For these reasons, developing a robust surrogate model at low computational cost is very challenging. The results presented in this study confirms that the non-intrusive spectral projection outperforms the regression based method. The non-intrusive spectral projection is found to produce the most accurate results at a considerable gain in the computational cost. Although the proposed algorithms were discussed within the context of acoustics, the conclusions drawn from this study are directly applicable to other wave applications. In practice, all the presented approach is equally useful for other wave applications.

Acknowledgment. The authors would like to thank anonymous referees for giving very helpful comments and suggestions that have greatly improved this paper.

References

[1] B. Barhoumi, J. Bessrour, An improved time-dependent boundary element method for two-dimensional acoustic problems in a subsonic uniform flow, Journal of Computational Science 21 (2017) 86 – 112.

[2] K. Li, W. Liao, An efficient and high accuracy finite-difference scheme for the acoustic wave equation in 3d heterogeneous media, Journal of Computational Science 40 (2020) 101063.

[3] H. Miguel, Apple acknowledges flaw in iphone signal meter, The New York Times July (2).

[4] N. El Moçayd, S. Ricci, N. Goutal, M. Rochoux, S. Boyaval, C. Goeury, D. Lucor, O. Thual, Polynomial surrogates for open-channel flows in random steady state, Environmental Modeling & Assessment 23 (2018) 309–331.

[5] G. Oliver, M. Antje, S. Hans-Jörg, U. Elisabeth, On the convergence of generalized polynomial chaos expansions, ESAIM: Mathematical Modelling and Numerical Analysis 46 (2) (2012) 317–339.

[6] M. Navacerrada, A. Pedrero, C. Díaz, Study of the uncertainty of façade sound insulation measurements: Analysis of the iso 12999-1 uncertainty proposal, Applied Acoustics 114 (2016) 1–9.

[7] A. Ndiaye, M. Bauerheim, S. Moreau, F. Nicoud, Uncertainty quantification of thermoacoustic instabilities in a swirled stabilized combustor, in: ASME Turbo Expo 2015: Turbine Technical Conference and Exposition, American Society of Mechanical Engineers Digital Collection, 2015.

[8] L. Magri, M. Bauerheim, F. Nicoud, M. Juniper, Stability analysis of thermo-acoustic nonlinear eigenproblems in annular combustors. part ii. uncertainty quantification, Journal of Computational Physics 325 (2016) 411–421.

[9] C. Silva, L. Magri, T. Runte, W. Polifke, Uncertainty quantification of growth rates of thermoacoustic instability by an adjoint helmholtz solver, Journal of Engineering for Gas Turbines and Power 139 (1).

[10] G. Poëtte, D. Lucor, Non intrusive iterative stochastic spectral representation with application to compressible gas dynamics, Journal of Computational Physics 231 (2012) 3587–3609.

[11] P. Roy, N. El Moçayd, S. Ricci, J. Jouhaud, N. Goutal, M. De Lozzo, M. Rochoux, Comparison of polynomial chaos and gaussian process surrogates for uncertainty quantification and correlation estimation of spatially distributed open-channel steady flows, Stochastic Environmental Research and Risk Assessment (2017) 1–19.

[12] J. Cheng, J. Wang, X. Wu, S. Wang, An improved polynomial-based nonlinear variable importance measure and its application to degradation assessment for high-voltage transformer under imbalance data, Reliability Engineering & System Safety 185 (2019) 175–191.

[13] M. El-Amrani, M. Seaid, A spectral stochastic semi-Lagrangian method for convection-diffusion equations with uncertainty, Journal of Scientific Computing 39 (2009) 371–393.

[14] R. Ghanem, D. Higdon, H. Owhadi, Handbook of uncertainty quantification, Vol. 6, Springer, 2017.

[15] M. Berveiller, B. Sudret, M. Lemaire, Stochastic finite element: a non intrusive approach by regression, European Journal of Computational Mechanics/Revue Européenne de Mécanique Numérique 15 (2006) 81–92.

[16] G. Blatman, B. Sudret, Adaptative sparse polynomial chaos expansion based on Least Angle Regression, Journal of Computational Physics 230 (2011) 2345–2367.

[17] X. Ma, N. Zabaras, An adaptive high-dimensional stochastic model representation technique for the solution of stochastic partial differential equations, Journal of Computational Physics 229 (10) (2010) 3884–3915.

[18] M. Raisee, D. Kumar, C. Lacor, A non-intrusive model reduction approach for polynomial chaos expansion using proper orthogonal decomposition, International Journal for Numerical Methods in Engineering 103 (2015) 293–312.

[19] G. Blatman, B. Sudret, Principal component analysis and Least Angle Regression in spectral stochastic finite element analysis, in: M. Faber, J. Köhler, K. Nishijima (Eds.), Proc. 11th Int. Conf. on Applications of Stat. and Prob. in Civil Engineering (ICASP11), Zurich, Switzerland, 2011.

[20] M. Chevreuil, A. Nouy, Model order reduction based on proper generalized decomposition for the propagation of uncertainties in structural dynamics, International Journal for Numerical Methods in Engineering 89 (2012) 241–268.

[21] N. El Moayd, M. Mohamed, D. Ouazar, M. Seaid, Stochastic model reduction for polynomial chaos expansion of acoustic waves using proper orthogonal decomposition, Reliability Engineering & System Safety 195 (2020) 106733.

[22] A. Resmini, J. Peter, D. Lucor, Sparse grids-based stochastic approximations with applications to aerodynamics sensitivity analysis, Int. J. Numer. Meth. Engng 10.1002/nme.5005.

[23] A. Clment, C. Soize, J. Yvonnet, Uncertainty quantification in computational stochastic multiscale analysis of nonlinear elastic materials, Computer Methods in Applied Mechanics and Engineering 254 (2013) 61 – 82.

[24] P. Lermusiaux, J. Xu, C. Chen, S. Jan, L. Chiu, Y. Yang, Coupled oceanacoustic prediction of transmission loss in a continental shelfbreak region: Predictive skill, uncertainty quantification, and dynamical sensitivities, IEEE Journal of Oceanic Engineering 35 (4) (2010) 895–916.

[25] T. Kuhn, J. Drrwchter, F. Meyer, A. Beck, C. Rohde, C. Munz, Uncertainty quantification for direct aeroacoustic simulations of cavity flows, Journal of Theoretical and Computational Acoustics 27 (01) (2019) 1850044.

[26] R. Hiptmair, L. Scarabosio, C. Schillings, C. Schwab, Large deformation shape uncertainty quantification in acoustic scattering, Advances in Computational Mathematics 44 (5) (2018) 1475–1518.

[27] F. Ihlenburg, I. Babuška, Finite element solution of the Helmholtz equation with high wave number Part i: The h-version of the FEM, Computers & Mathematics with Applications 30 (1995) 9–37.

[28] I. M. Babuska, S. Sauter, Is the pollution effect of the fem avoidable for the helmholtz equation considering high wave numbers?, SIAM Journal on numerical analysis 34 (6) (1997) 2392–2423.

[29] G. Diwan, M. Mohamed, Pollution studies for high order isogeometric analysis and finite element for acoustic problems, Computer Methods in Applied Mechanics and Engineering 350 (2019) 701–718.

[30] A. Lieu, G. Gabard, H. Bériot, A comparison of high-order polynomial and wave-based methods for helmholtz problems, Journal of Computational Physics 321 (2016) 105–125.

[31] K. Christodoulou, O. Laghrouche, M. Mohamed, J. Trevelyan, High-order finite elements for the solution of helmholtz problems, Computers & Structures 191 (2017) 129–139.

[32] A. El Kacimi, O. Laghrouche, M. Mohamed, J. Trevelyan, Bernstein-bézier based finite elements for efficient solution of short wave problems, Computer Methods in Applied Mechanics and Engineering 343 (2019) 166–185.

[33] I. Babuška, J. Melenk, The partition of unity method, International journal for numerical methods in engineering 40 (4) (1997) 727–758.

[34] O. Laghrouche, P. Bettess, R. Astley, Modelling of short wave diffraction problems using approximating systems of plane waves, International Journal for Numerical Methods in Engineering 54 (10) (2002) 1501–1533.

[35] T. Strouboulis, R. Hidajat, I. Babuška, The generalized finite element method for helmholtz equation. part ii: Effect of choice of handbook functions, error due to absorbing boundary conditions and its assessment, Computer Methods in Applied Mechanics and Engineering 197 (5) (2008) 364–380.

[36] M. Mohamed, O. Laghrouche, A. El-Kacimi, Some numerical aspects of the pufem for efficient solution of 2d helmholtz problems, Computers & structures 88 (23-24) (2010) 1484–1491.

[37] T. Okuzono, M. Mohamed, K. Sakagami, Potential of room acoustic solver with plane-wave enriched finite element method, Applied Sciences 10 (6) (2020) 1969.

[38] T. Zhou, J. Chazot, E. Perrey-Debain, L. Cheng, Partition of unity finite element method for the modelling of acoustic black hole wedges, Journal of Sound and Vibration (2020) 115266.

[39] M. Dinachandra, S. Raju, Plane wave enriched partition of unity isogeometric analysis (puiga) for 2d-helmholtz problems, Computer Methods in Applied Mechanics and Engineering 335 (2018) 380–402.

[40] M. Mahmood, O. Laghrouche, J. Trevelyan, A. El Kacimi, Implementation and computational aspects of a 3d elastic wave modelling by pufem, Applied Mathematical Modelling 49 (2017) 568–586.

[41] A. El Kacimi, O. Laghrouche, Numerical modelling of elastic wave scattering in frequency domain by the partition of unity finite element method, International journal for numerical methods in engineering 77 (12) (2009) 1646–1669.

[42] C. Lu, B. Shanker, Generalized finite element method for vector electromagnetic problems, IEEE transactions on antennas and propagation

55 (5) (2007) 1369–1381.

[43] T. Zhou, J. Chazot, E. Perrey-Debain, L. Cheng, Performance of the partition of unity finite element method for the modeling of timoshenko beams, Computers & Structures 222 (2019) 148–154.

[44] M. Drolia, M. Mohamed, O. Laghrouche, M. Seaid, J. Trevelyan, Enriched finite elements for initial-value problem of transverse electromagnetic waves in time domain, Computers & Structures 182 (2017) 354–367.

[45] M. Drolia, M. Mohamed, O. Laghrouche, M. Seaid, A. El Kacimi, Explicit time integration with lumped mass matrix for enriched finite elements solution of time domain wave problems, Applied Mathematical Modelling 77 (2020) 1273–1293.

[46] J. Jiang, M. Mohamed, M. Seaid, H. Li, Identifying the wavenumber for the inverse Helmholtz problem using an enriched finite element formulation, Computer Methods in Applied Mechanics and Engineering 340 (2018) 615–629.

[47] S. Petersen, C. Farhat, R. Tezaur, A space–time discontinuous galerkin method for the solution of the wave equation in the time domain, International journal for numerical methods in engineering 78 (3) (2009) 275–295.

[48] D. Wang, R. Tezaur, C. Farhat, A hybrid discontinuous in space and time galerkin method for wave propagation problems, International Journal for Numerical Methods in Engineering 99 (4) (2014) 263–289.

[49] R. Hiptmair, A. Moiola, I. Perugia, A survey of trefftz methods for the helmholtz equation, in: Building bridges: connections and challenges in modern approaches to numerical partial differential equations, Springer, 2016, pp. 237–279.

[50] N. Wiener, The homogeneous chaos, Am.J.Math 60 (1938) 897–936.

[51] P. Spanos, R. Ghanem, Stochastic Finite Elements: A Spectral Approach, Springer, 1991.

[52] D. Xiu, G. E. Karniadakis, Modeling uncertainty in flow simulations via generalized polynomial chaos, Journal of Computational Physics 187 (2003) 137–167.

[53] D. Xiu, Numerical methods for stochastic computations: a spectral method approach, Princeton university press, 2010.

[54] R. Cameron, W. Martin, The orthogonal development of non-linear functionals in series of fourier-hermite functionals, Annals of Mathematics (1947) 385–392.

[55] S. Choi, R. Grandhi, R. Canfield, C. Pettit, Polynomial Chaos expansion with Latin Hypercube Sampling for estimating response variability, AIAA journal 42 (6) (2004) 1191–1198.

[56] G. Casella, E. George, Explaining the Gibbs sampler, The American Statistician 46 (1992) 167–174.

[57] A. Smith, G. Roberts, Bayesian computation via the Gibbs sampler and related markov chain Monte Carlo methods, Journal of the Royal Statistical Society: Series B (Methodological) 55 (1993) 3–23.

[58] Q. Liu, D. A. Pierce, A note on gauss-hermite quadrature, Biometrika 81 (3) (1994) 624–629.

[59] M. Abramowitz, I. A. Stegun, Handbook of mathematical functions with formulas, graphs, and mathematical tables, Vol. 55, US Government printing office, 1970.

[60] I. Arasaratnam, S. Haykin, R. J. Elliott, Discrete-time nonlinear filtering algorithms using gausshermite quadrature, Proceedings of the IEEE 95 (5) (2007) 953–977.

[61] N. El Moçayd, La décomposition en polynômes du chaos pour lámélioration de lássimilation de données ensembliste en hydraulique fluviale, PhD Université de Toulouse, INP.

[62] B. Sudret, Global sensitivity analysis using polynomial chaos expansion, "Reliability Engineering & System Safety" 93 (2008) 964–979.

[63] M. Baudin, A. Dutfoy, B. Iooss, A. Popelin, Openturns: An industrial software for uncertainty quantification in simulation, Handbook of uncertainty quantification (2017) 2001–2038.

[64] P. Karve, L. Kallivokas, L. Manuel, A framework for assessing the uncertainty in wave energy delivery to targeted subsurface formations, Journal of applied geophysics 125 (2016) 26–36.

[65] J. Vrugt, P. Stauffer, T. Wöhling, B. Robinson, V. Vesselinov, Inverse modeling of subsurface flow and transport properties: A review with new developments, Vadose Zone Journal 7 (2) (2008) 843–864.

[66] R. E. Caflisch, Monte carlo and quasi-monte carlo methods, Acta Numerica 7 (1998) 149.

[67] A. Fahim, G. Saake, A. Salem, F. Torkey, M. Ramadan, K-means for spherical clusters with large variance in sizes, World Academy of

Science, Engineering and Technology, International Journal of Computer, Electrical, Automation, Control and Information Engineering 2 (2008) 2923–2928.

[68] X. Chen, Z. J. Wang, M. J. McKeown, Asymptotic analysis of robust lassos in the presence of noise with large variance, IEEE Transactions on Information Theory 56 (10) (2010) 5131–5149.

[69] W. Feller, P. M. Morse, An introduction to probability theory and its applications, PhT 11 (4) (1958) 32.

[70] B. Efron, Bootstrap Methods: Another Look at the Jackknife, Springer New York, New York, NY, 1992, pp. 569–593.

[71] W. J. Morokoff, R. E. Caflisch, Quasi-monte carlo integration, Journal of Computational Physics 122 (2) (1995) 218 – 230.

[72] I. Sobol, On quasi-monte carlo integrations, Mathematics and Computers in Simulation 47 (2) (1998) 103 – 112.

[73] H. Chi, M. Mascagni, T. Warnock, On the optimal halton sequence, Mathematics and Computers in Simulation 70 (1) (2005) 9 – 21.

[74] G. Migliorati, F. Nobile, Analysis of discrete least squares on multivariate polynomial spaces with evaluations at low-discrepancy point sets, Journal of Complexity 31 (4) (2015) 517 – 542.